IEEE Photonics Journal
An IEEE Photonics Society Publication

Open Access

Plasmonic Structural-Color Thin Film With a Wide Reception Angle and Strong Retro-Reflectivity

Volume 4, Number 6, December 2012

Inchul Woo
Sunkyu Yu
Jae Sung Lee
Jung H. Shin
Mi Jung
Namkyoo Park

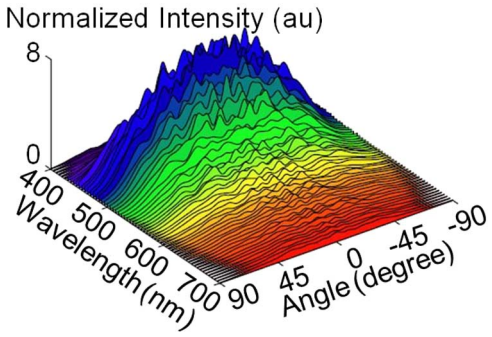

DOI: 10.1109/JPHOT.2012.2229973
1943-0655/$31.00 ©2012 IEEE

IEEE photonics SOCIETY

IEEE

Plasmonic Structural-Color Thin Film With a Wide Reception Angle and Strong Retro-Reflectivity

Inchul Woo,[1] Sunkyu Yu,[1] Jae Sung Lee,[1] Jung H. Shin,[2] Mi Jung,[3] and Namkyoo Park[1]

[1]Photonic Systems Laboratory, School of EECS, Seoul National University, Seoul 151-742, Korea
[2]Department of Phys./Graduate School of Nanoscience and Technology, KAIST, Daejeon, South Korea
[3]Sensor System Research Center, KIST, Seoul 136-791, Korea

DOI: 10.1109/JPHOT.2012.2229973
1943-0655/$31.00 ©2012 IEEE

Manuscript received October 4, 2012; revised November 19, 2012; accepted November 19, 2012. Date of current version November 29, 2012. This work was supported by the National Research Foundation (GRL, K20815000003; Center for Subwavelength Optics, SRC 2008-0662256) and by the Global Frontier Program (2011-0031561). J. H. Shin acknowledges support from MEST (2011-0029868). Corresponding author: N. Park (e-mail: nkpark@snu.ac.kr).

Abstract: We propose a plasmonic structural color in the form of a thin film with a monolayer of randomly dispersed silver nanoshells. By employing spatially isotropic optical dipole antenna nanoshells to achieve efficient couplings to obliquely incident field and by utilizing local frustration and interference of randomly dispersed scatterer phases, we successfully introduce plasmonic-driven unique traits of retro-reflection as an example of a plasmonic structural color. As compared to the natural counterpart, *Morpho rhetenor*, a much wider reception angle, up to 70°, and a stronger retro-reflectivity of 35–45% are achieved.

Index Terms: Nanophotonics, resonance light scattering.

1. Introduction

Structural colors, often observed in nature, such as in the wings of butterflies and peacocks, have stimulated scientific interests for well over a century. The hue is often variable with the angle of view, and the color is not affected by photo-bleaching processes. The structural color can be changed or even eliminated by altering the refractive index of the surrounding medium. There exist different mechanisms for structural colorations in relation to photonic crystals (*Metapocyrtus* weevil), diffraction grating (*Ostracod* crustacean), scattering structures (nanoparticle colloid), or multilayer reflections (*Ovalipes molleri*) [1], [2]. Structural colors, each with distinct properties, such as color tunability [3]–[6], wide viewing angles [7]–[14], or retro-reflection properties [11]–[15], have been reported or artificially demonstrated. In terms of wide viewing angle, *Morpho* butterflies of the multilayer reflections also have received added attentions. There are many biomimetic realizations of artificial structural colors with a wide viewing angle and color stability comparable to or exceeding that of the *Morpho* [7]–[10], but in most cases, dielectric materials only have been used in their construction. Structural colors utilizing plasmonic advantages—strong coupling with light [16] and flexibility in spectral and polarization control supported by diverse morphologies [17]–[19]—could be imagined but have not treated until recently [20]. By utilizing aperiodic and randomly dispersed pinwheel nanoparticles on top of gold film, isotropic coloration of metal films was demonstrated.

In this paper, we propose a plasmonic structural color, specifically in the form of a monolayer of silver nanoshells randomly dispersed in a low-index thin film, and analyze its spectral properties,

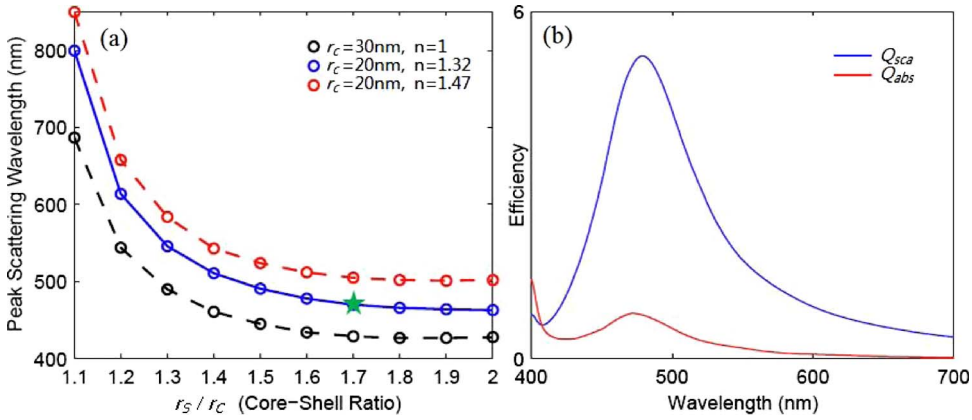

Fig. 1. (a) Peak scattering wavelengths of the 3-D SiO_2-Ag nanoshells as a function of the core-shell radius ratio (r_s/r_c), in different host matrices. The design point is marked with a green star. (b) Scattering/absorption efficiencies of the 2-D shell of $(r_c, r_s) = (20\ \text{nm}, 34\ \text{nm})$ in host matrix of $n = 1.32$.

focusing on its plasmonic-driven characteristics. Each plasmonic particle acting as a spectrally and spatially well-defined optical antenna, their inherited advantages—such as a simple unit cell of coloration, a sharp color selectivity, and a large scattering cross section—are expected, as confirmed in this study. Further, we also show that, by utilizing a plasmonic nanoshell antenna with an isotropic dipole response, a very efficient coupling to oblique-incident fields (up to $\sim 70^\circ$) and a strong retro-reflectivity (35–45%) can be obtained, as compared to the natural counterpart, *Morpho rhetenor* (~15%, 30°) [13], [14]. Design principles, including the effect of nanoshell scattering cross section and randomness in particle dispersion, in relation to the viewing angle and retro-reflection properties are also discussed with *2-D* and *3-D* particle realizations.

2. Design Principles and Viewing Angle Analysis

To define the color, a spherical particle was selected to support dipole modes, considering both the spatial isotropy and the spectral selectivity near the target spectrum [17]–[19]. Specifically, here we focus on a silica-silver shell because its resonance is tunable over the visible range, and as it has a smaller absorption cross section C_{abs} than those of solid spheres. The finite element method (COMSOL) was used to calculate the scattering cross section C_{sca} [21], [22], with triangular grids ($< \lambda/100$ in metal) and perfectly matched layers, and the Ag parameters from reference [22]. Fig. 1(a) shows the peak scattering wavelength of the *3-D* SiO_2-Ag shells as a function of the core-shell radius ratio r_s/r_c, in host materials of refractive index n. A *3-D* shell of $(r_c, r_s) = (20\ \text{nm}, 34\ \text{nm})$ in a medium of MY-132 ($n = 1.32$, [23]) was selected considering the tolerance in particle synthesis and spectrum (480 nm, *Morpho rhetenor* [11]).

Before working on the structural color of the *3-D*-shell (in Section 4), in order to study the underlying physics, we analyze the case of a *2-D* shell first. The radius of a *2-D* shell was set to be equal to that of the *3-D* shell [24]–[26]. Fig. 1(b) shows the scattering efficiency Q_{sca} of the *2-D* shell at the peak wavelength of 479 nm. Given the numerically obtained $Q_{\text{sca}} = 5.23$ and the scattering cross section C_{sca} $(= 2r_s \cdot Q_{\text{sca}} = 356\ \text{nm})$, the optimum inter-particle distance d $(= C_{\text{sca}} - 2r_s)$—virtually free from dipole-dipole couplings—was estimated to be 288 nm. Considering the voids of particle and margins for the randomness in particle dispersion, a smaller d of 250 nm was selected. It should be noted that, with this choice of d, a *monolayer* of particles was sufficient to provide a near theoretical maximum reflectivity and, also, a sharp spectrum.

Upon the determination of particle size and optimum inter-particle distance, we studied the effect of local interference of scatterer phases—by introducing a parameter σ to account for the randomness in particle dispersion [of Gaussian distribution both in horizontal (σ_x) and vertical (σ_z) directions, Fig. 2(a)]. For the film fabrication, a self-assembled monolayer of metallic shells mixed with dielectric spheres of predetermined randomness in their size could be utilized, with subsequent

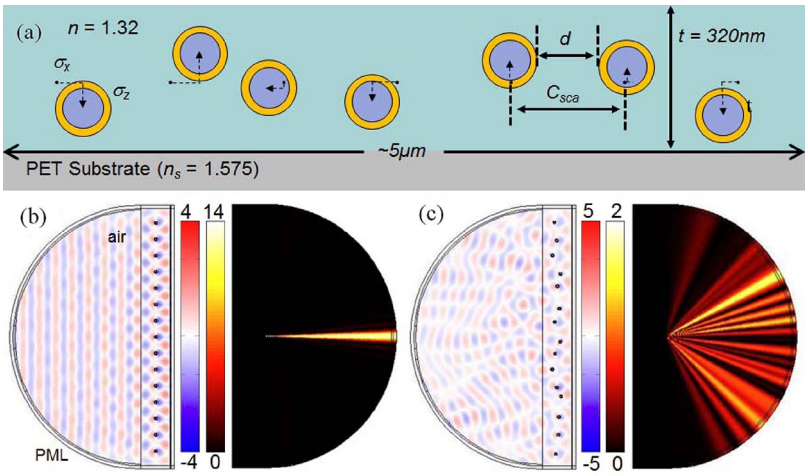

Fig. 2. (a) Schematic of the plasmonic structural color. σ_x, σ_z: randomness in particle dispersion; d: inter-particle distance; t: film thickness; and (b) and (c) show near- (left) and far- (right) field reflection patterns of regular $(\sigma_x, \sigma_z = 0$ nm$)$ and irregular $(\sigma_x, \sigma_z = 50$ nm$)$ array of nanoshells.

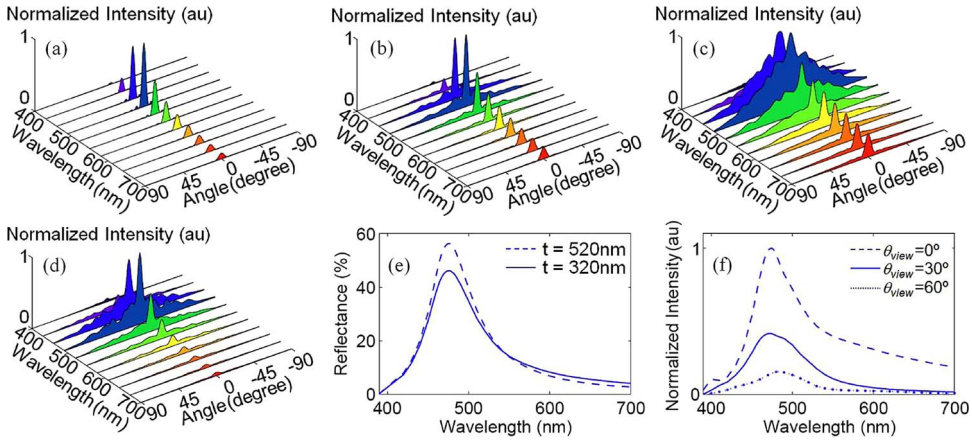

Fig. 3. Film responses for the normal incidence of light illumination. Reflection intensity spectra from the particle array as a function of the viewing angle and particle dispersion (a) $\sigma = 0$ nm; (b) $\sigma = 30$ nm; and (c) $\sigma = 50$ nm, respectively. $t = 320$ nm; (d) reflection spectra for $t = 520$ nm and $\sigma = 50$ nm. (e) comparison of total reflectance spectra for different film thickness ($t = 520$ nm, and 320 nm). $\sigma = 50$ nm. (f) reflection intensity spectra measured at different viewing angles.

low-temperature annealing. A regularly [Fig. 2(b)] and randomly [Fig. 2(c), $\sigma_{x,z} = 50$ nm] dispersed nanoshell array (as shown in the rectangular box next to the left semicircles) and its near- and far-field patterns (left and right semicircles) are illustrated. The far-field patterns were calculated using the COMSOL-embedded Stratton-Chu formula, for normally incident plane waves (TM, $\lambda = 476$ nm). With the interference of phases from the randomly dispersed scatterers, the enhancement of viewing angle is evident [27], in comparison with the highly directional reflection from a regularly dispersed nanoshell film.

Fig. 3(a)–(c) shows the effects of dispersion σ, as a function of *viewing* angle θ_{view} and λ—for the normal incidence of light. Each reflection intensity spectrum was obtained by averaging the responses from 30 film sets. To note, each film was realized with fifteen scatterers of random dispersion σ, spread over the lateral dimension $\gg \lambda$ (here, $\sim 10\lambda$ with 15 particles). Integrating the reflected intensities over θ_{view}, the total reflectivity spectrum R was calculated [Fig. 3(e), $\Delta\lambda =$ 5 nm, 400–700 nm]. With the increase of σ, the increase of $\Delta\theta_{\text{view}}$ within the bandwidth of particle

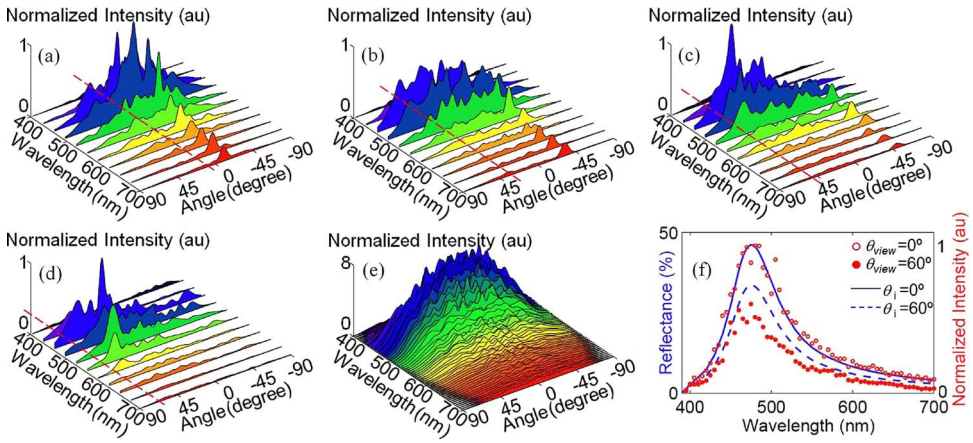

Fig. 4. Reflection spectra of the film $(\sigma = 50\ \text{nm}; t = 320\ \text{nm})$, for illumination angles of (red dashed line) (a) $\theta_i = 10°$; (b) $\theta_i = 30°$; (c) $\theta_i = 50°$; and (d) $\theta_i = 70°$; and (e) reflection spectra for diffusive illumination; and (f) blue lines: total reflectance spectra for different illumination angles. red marks: reflection spectra measured at different viewing angles (diffusive excitation).

resonance was observed, as saturating after $\sigma = 50$ nm. It is worth mentioning that the film thickness t was set to 320 nm to suppress the 0° Fabry–Perot reflection from the film [$t = 520$ nm, Fig. 3(d) and (e)]. A successful *2-D* replication of the color and peak reflectivity ($\lambda = 476$ nm; $R = 46\%$) of *Morpho rhetenor* (480 nm, 47%) was made, in addition to superior color selectivity ($\Delta\lambda = 73$ nm, full width half maximum) and a wider viewing angle ($\Delta\theta_{\text{view}} = 114°$, at 5^{-1} intensity) with good color stability [Fig. 3(f)], when compared to those of *Morpho rhetenor* ($\Delta\lambda = 150$ nm, $\Delta\theta_{\text{view}} \sim 80°$) [11]–[14].

3. Response On Oblique Illumination and Retro-Reflection Properties

To further study the behavior of plasmonic structural color, the film response as a function of *oblique illumination* ($\theta_i \neq 0$) of light also has been analyzed. Fig. 4(a)–(d) shows the reflection spectra of the film $(\sigma = 50\ \text{nm}; t = 320\ \text{nm})$, calculated for $\theta_i = 10{-}70°$ in 20° steps. Strong reflection over large viewing angle $\Delta\theta_{\text{view}}$ was obtained with negligible dependence to illumination angle θ_i [Fig. 4(a)–(d)], promoted by the large scattering cross section and spatial isotropy of the *plasmonic* nanoantenna. Taking a normalized sum ($\sum R(\theta_i)$, each $R(\theta_i)$ obtained for $\theta_i = 10{-}170°$ in 10° steps), the spectral response of the film for a *diffusive illumination* has been also calculated [Fig. 4(e)]. The total reflectance of the film was 40%.

It is critical to note the signature of strong retro-reflection ($\theta_r \approx \theta_i$) in Fig. 4(a)–(d) ($\theta_i$ marked with red dashed lines). With the plasmon *dipole* resonance of the isotropic nanoshell, the re-radiated fields propagate back to the incident direction, over a wide angle of θ_i. A large illumination *reception angle* $\theta_{ir} \sim 70°$, defined by $R(\theta_{ir}) \equiv 0.5 \cdot R(\theta_i = 0)$ [13], was obtained. In Fig. 4(f), the strong reflectance $R(\theta_i)$ over large variation of θ_i (blue lines) and spectral stability at different viewing angle θ_{view} (red marks, measured for diffusive excitation) are also evident. Fig. 5 compares the far-field reflection patterns of the regularly and randomly dispersed nanoshell film in polar coordinates for four illumination angles (rainbow arrows: $0 \sim 60°$). For regularly dispersed particle films [Fig. 5(a)–(d)], very specular, diffraction-limited ($\theta_{m=0}$ and $\theta_{m=1}$. m: diffraction order), and highly directional reflection was observed. To compare, for the randomly dispersed particle films [Fig. 5(e)–(h)], with the introduction of σ, a much stronger and wider angle retro-reflection from quasi-isolated particles was observed. The reduction of grating diffraction was more sensitive to the in-plane particle dispersion σ_x; meanwhile, the retro-reflection was strongly dependent on the out-of-plane dispersion σ_z. It is worthwhile to mention that the wavelength dependence of retro-reflection is pronounced near the dipole resonance (476 nm, blue lines) of the nanoshell. As well, in the near-field pattern (Fig. 5, rectangular box under each semicircle), the incident-angle aligned retro-radiation from the dipole of quasi-isolated nanoshells was evident. Compared to the peak retro-reflectivity of

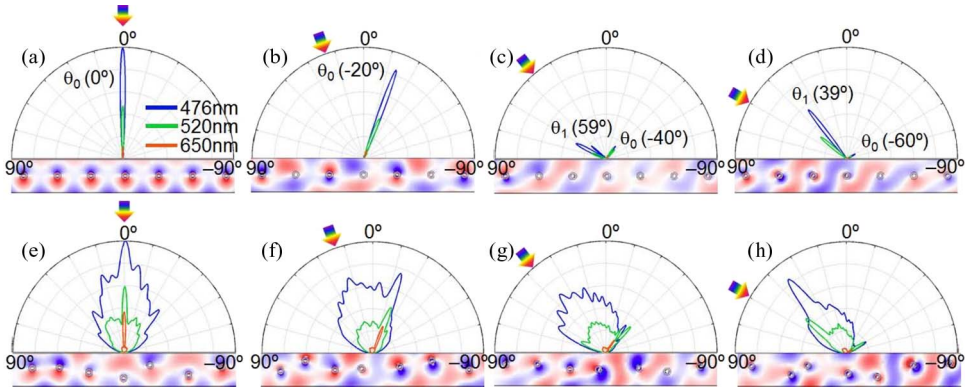

Fig. 5. Far-field distributions of scattered waves for different light illumination angles to the film. Nanoshell dispersion and their near-field patterns are shown in the rectangular box under each semicircle. $\lambda = 476$ nm. Cases of (a–d) regularly and (e–h) irregularly dispersed particles are compared for illumination angles of $\theta_i = 0°$, 20°, 40°, and 60°, respectively. Strong retro-reflections are evident for the cases of randomly dispersed $(\sigma = 50$ nm$)$ plasmonic particle arrays.

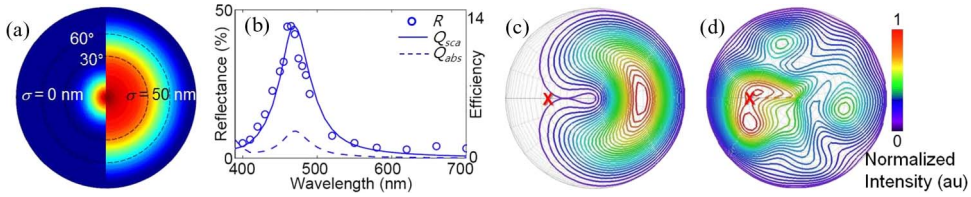

Fig. 6. (a) Far-field reflections seen from the top surface of the radiation sphere, for plasmonic films of 3-D nanoshell. $\sigma = 0$ nm (left) and $\sigma = 50$ nm (right). (b) total reflectance spectrum (circles) of the $\sigma = 50$ nm film, overlaid to the scattering and absorption efficiency of an isolated nanoshell. (c) and (d) show the far-field reflected intensities (17 film realizations averaged) for an obliquely-incident light $(\theta_i = 40°)$, respectively for a regularly $(\sigma = 0$ nm$)$ and a randomly $(\sigma = 50$ nm$)$ dispersed 3-D nanoshell array.

Morpho rhetenor (∼15%, at $\theta_{ir} \sim 30°$ [13], [14], the measured retro-reflectivity from the randomly dispersed nanoshell array was much higher ($R = 35{-}45\%$ for $\theta_i = 0 \sim 50°$), with a much bigger reception angle $(\theta_{ir} = 70°)$.

4. Extension To *3-D* Nanoshell Plasmonic Structural Color

With the physical insights developed from the *2-D* analysis, we now extend our study to the case of a *3-D* nanoshell plasmonic structural color. Since a *3-D* shell of $(r_c, r_s) = (20$ nm, 34 nm$)$ has a larger value of $Q_{sca} = 13$ [at $\lambda = 470$ nm, Fig. 6(b)] than a *2-D* shell, it is required to recalculate the theoretical-optimum inter-particle distance $(d = 2 \cdot (\pi r^2 \cdot Q_{sca}/\pi)^{0.5} - 2r_s = 178$ nm$)$. Again, considering voids in the array and margins for the random dispersion, d was set to 172 nm in the *3-D* particle film analysis. A total of nineteen *3-D* nanoshells and seventeen film realizations were used to attain sufficient averaging and dispersion randomness. As can be seen in Fig. 6(a), a wider viewing angle $\Delta\theta_{view}$ (seen from film top) for the case of random particle dispersion ($\sigma_{x,y,z} = 50$ nm along each of the three axes simultaneously, $\theta_i = 0°$, right semicircle) was evident, compared to that of the regular array (left semicircle). High reflectivity of $R = 45\%$ and excellent color selectivity $(\Delta\lambda = 50$ nm$)$ were obtained from the randomly dispersed *3-D* particle array, which is close to the theoretical maximum values [Fig. 6(b)]. Fig. 6(c) and (d) also compares the retro-reflection properties from the regularly and randomly dispersed particle films, for an oblique incidence angle of 40° (marked with red cross). Compared to the strong spectral reflection and the negligible retro-reflection from the regular array film, strong retro-reflection $(R = 38\%)$ from the *3-D* plasmonic structural color was observed, in line with the result from the *2-D* analysis.

5. Conclusion

In this paper, we proposed a structural-color utilizing plasmonic antenna as a base element, in the form of a monolayer of randomly dispersed silver nanoshells in a low-index thin film. By using a unit cell of structural color made of a spectrally/spatially well-defined plasmonic shell and by employing local frustration/interference of randomly dispersed scatterer phases, it was possible to achieve a wide viewing angle, high reflectance ($R = 45\%$), and excellent color selectivity ($\Delta\lambda = 50{-}70$ nm; $\lambda = 470$ nm). With the frustration of phase interference between the nanoshell optical antenna, the isotropic dipole retro-radiation of an isolated nanoshell is recovered for a film of particle random dispersion; a strong resonance-enhanced retro-reflection ($R_{\text{retro}} = 35{-}45\%$) and a large illumination reception angle $\theta_{ir} \sim 70^{\circ}$ were possible. Even if the present demonstration was focused on retro-reflection properties derived from an isotropic dipole antenna, the outlined procedure would not exclude the possibilities of other plasmonic structural colors of exotic properties, for example, using nanoparticles of multimodal, chiral, or anisotropic properties and controllable inter-particle coupling interactions.

References

[1] A. R. Parker and N. Martini, "Structural colour in animals—Simple to complex optics," *Opt. Laser Technol.*, vol. 38, no. 4–6, pp. 315–322, Jun.–Sep. 2006.

[2] D. G. Stavenga1, S. Stowe, K. Siebke, J. Zeil, and K. Arikawa, "Butterfly wing colours: Scale beads make white pierid wings brighter," *Proc. R. Soc. Lond. B, Math. Biol. Sci.*, vol. 271, no. 1548, pp. 1577–1584, Aug. 2004.

[3] J. Wang, Y. Wen, H. Ge, Z. Sun, Y. Zheng, Y. Song, and L. Jiang, "Simple fabrication of full color colloidal crystal films with tough mechanical strength," *Macromol. Chem. Phys.*, vol. 207, no. 6, pp. 596–604, Mar. 2006.

[4] A. C. Arsenault, T. J. Clark, G. V. Freymann, L. Cademartiri, R. Sapienza, J. Bertolotti, E. Vekris, S. Wong, V. Kitaev, I. Manners, R. Z. Wang, S. John, D. Wiersma, and G. A. Ozin, "From colour fingerprinting to the control of photoluminescence in elastic photonic crystals," *Nature Mater.*, vol. 5, no. 3, pp. 179–184, Mar. 2006.

[5] H. Fudouzi and Y. Xia, "Colloidal crystals with tunable colors and their use as photonic papers," *Langmuir*, vol. 19, no. 23, pp. 9653–9660, Nov. 2003.

[6] A. C. Arsenault, D. P. Puzzo, I. Manners, and G. A. Ozin, "Photonic-crystal full-colour displays," *Nature Photon.*, vol. 1, no. 8, pp. 468–472, Aug. 2007.

[7] K. Watanabe, T. Hoshino, K. Kanda, Y. Haruyama, and S. Matsui, "Brilliant blue observation from a morpho-butterfly-scale quasi-structure," *Jpn. J. Appl. Phys.*, vol. 44, no. 1, pp. L48–L50, Jan. 2005.

[8] A. Saito, Y. Miyamura, M. Nakajima, Y. Ishikawa, K. Sogo, Y. Kuwahara, and Y. Hirai, "Reproduction of the Morpho blue by nanocasting lithography," *J. Vac. Sci. Technol. B, Microelectron. Nanometer Struct.*, vol. 24, no. 6, pp. 3248–3251, Nov. 2006.

[9] T. S. Kustandi, H. Y. Low, J. H. Teng, I. Rodriguez, and R. Yin, "Mimicking domino-like photonic nanostructures on butterfly wings," *Small*, vol. 5, no. 5, pp. 574–578, Mar. 2009.

[10] K. Chung, S. Yu, C. Heo, J. W. Shim, S. Yang, M. Han, H. Lee, Y. Jin, S. Y. Lee, N. Park, and J. H. Shin, "Flexible, angle-independent structural color reflectors inspired by morpho butterfly wings," *Adv. Mater.*, vol. 24, no. 18, pp. 2375–2379, May 2012.

[11] P. Vukusic, J. R. Sambles, C. R. Lawrence, and R. J. Wootton, "Quantified interference and diffraction in single Morpho butterfly scales," *Proc. R. Soc. Lond. B, Math. Biol. Sci.*, vol. 266, no. 1427, pp. 1403–1411, Jul. 1999.

[12] S. Kinoshita, S. Yoshioka, Y. Fujii, and N. Okamoto, "Photophysics of structural color in the Morpho butterflies," *Forma*, vol. 17, no. 2, pp. 103–121, 2002.

[13] L. Plattner, "Optical properties of the scales of Morpho rhetenor butterflies: Theoretical and experimental investigation of the back-scattering of light in the visible spectrum," *Proc. R. Soc. Interface*, vol. 1, no. 1, pp. 49–59, Nov. 2004.

[14] M. Kambe, D. Zhu, and S. Kinoshita, "Origin of retroreflection from a wing of the Morpho butterfly," *J. Phys. Soc. Jpn.*, vol. 80, no. 5, pp. 054801-1–054801-10, May 2011.

[15] M. Kolle, P. M. Salgard-Cunha, M. R. J. Scherer, F. Huang, P. Vukusic, S. Mahajan, J. J. Baumberg, and U. Steiner, "Mimicking the colourful wing scale structure of the Papilio blumei butterfly," *Nature Nanotechnol.*, vol. 5, no. 7, pp. 511–515, Jul. 2010.

[16] C. F. Bohren and D. R. Huffman, *Absorption and Scattering of Light by Small Particles*. New York: Wiley, 1983.

[17] J. L. West and N. J. Halas, "Engineered nanomaterials for biophotonics applications: Improving sensing, imaging, and therapeutics," *Annu. Rev. Biomed. Eng.*, vol. 5, no. 1, pp. 285–292, Aug. 2003.

[18] K. L. Kelly, E. Coronado, L. L. Zhao, and G. C. Schatz, "The optical properties of metal nanoparticles: The influence of size, shape, and dielectric environment," *J. Phys. Chem. B*, vol. 107, no. 3, pp. 668–677, Jan. 2003.

[19] E. Prodan, C. Radloff, N. J. Halas, and P. Nordlander, "A hybridization model for the plasmon response of complex nanostructures," *Science*, vol. 302, no. 5644, pp. 419–422, Oct. 2003.

[20] S. Y. Lee, C. Forestiere, A. J. Pasquale, J. Trevino, G. Walsh, P. Galli, M. Romagnoli, and L. D. Negro, "Plasmon-enhanced structural coloration of metal films with isotropic Pinwheel nanoparticle arrays," *Opt. Exp.*, vol. 19, no. 24, pp. 23 818–23 830, Nov. 2011.

[21] M. W. Knight and N. J. Halas, "Nanoshells to nanoeggs to nanocups: Optical properties of reduced symmetry core-shell nanoparticles beyond the quasistatic limit," *New J. Phys.*, vol. 10, no. 10, p. 105 006, Oct. 2008.

[22] P. B. Johnson and R. W. Christy, "Optical constants of the noble metals," *Phys. Rev. B, Condens. Matter Mater. Phys.*, vol. 6, no. 12, pp. 4370–4379, Dec. 1972.
[23] [Online]. Available: http://www.mypolymers.com/
[24] K. Ehrhold, S. Christiansen, and U. Gosele, "Plasmonic properties of bimetal nanoshell cylinders and spheres," in *Proc. COMSOL Conf.*, Hanover, Germany, 2008, pp. 1–12.
[25] J. Li, X. Li, F. Yu, Y. Chen, and W. Huang, "Mechanism and analysis of structural color in two typical butterfly scales," in *Proc. IEEE 5th Int. Conf. Nano/Micro Eng. Mol. Syst.*, Xiamen, China, 2010, pp. 723–727.
[26] R. Taylor, F. Seifrt, O. Zhuromskyy, U. Peschel, G. Leugering, and W. Peukert, "Painting by numbers: Nanoparticle-based colorants in the post-empirical age," *Adv. Mater.*, vol. 23, no. 22/23, pp. 2554–2570, Jun. 2011.
[27] S. Kinoshita and S. Yoshioka, "Structural colors in nature: The role of regularity and irregularity in the structure," *ChemPhysChem*, vol. 6, no. 8, pp. 1442–1459, Aug. 2005.